Ultraoleophobicity of Thermally Oxidized Surfaces of C36000 Alloy

Aniedi E. Nyong[1] . Pradeep K. Rohatgi[2]

[1]Materials Chemistry Research Unit, Department of Chemistry, Akwa Ibom State University, Nigeria.
[2]Composite Research Center, Department of Materials Science and Engineering, University of Wisconsin-Milwaukee, United States of America.

ABSTRACT

The contact angle of oil at the water-oil interface has been studied on surfaces of thermally oxidized C36000 copper alloy. The chemical composition of the thermally oxidized C36000 alloy was determined through x-ray diffraction and energy dispersive x-ray analyses. The x-ray diffraction of the oxidized surfaces confirmed oxide crystallites, indexed as the (100), (002), (101), (102), (103) and (110) planes of the hexagonal ZnO. Using the Scherrer's formula, sizes of the ZnO crystallites were within the range of 36.30 nm to 86 nm for the alloy samples oxidized for 1, 2 and 3 hours in N_2/0.75 wt. % O_2 gaseous atmosphere and in air. The oxide layers for the alloy oxidized for 1 hour in the 0.75 wt. % O_2 gaseous atmosphere had a high density of oxide nanowires. The nanowire density was estimated as an average of 19 nanowires per μm^2, with the average length, average diameter and the average distance between the nanowires measured as 0.52 ± 0.31 μm, 34.0 ± 0.02 nm and 0.17 ± 0.07 nm respectively. The contact angles of oil at the oil-water interface showed maximum values of $113.9° \pm 1.9$ and $130.9° \pm 1.9°$ respectively after thermal oxidation for 3 hours N_2/0.75 wt. % O_2 gaseous atmosphere and in air. The contact angle of $130.9° \pm 1.9°$ confirmed ultraoleophobicity.

Introduction

The C36000 alloy is a leaded copper alloy containing copper, zinc and lead as the elemental components of its two phases [1]. The alloy consists of a 2-phase microstructure, the alpha and the beta phases; with the lead particles existing practically as insoluble particles dispersed within the microstructure [2-3]. The C36000 alloy has numerous uses, mostly in plumbing and as fixtures for water recticulation [4]. To that extent, the alloy comes in contact with fluids, such as different types of oils during its useful life-span, which could result in the fouling of its surfaces [5].

Prior to now, several workers have investigated the mechanism through which underwater oleophobicity/ superoleophobicity can be achieved [6-7]. Other specific instances of previous work on the wetting of thermally oxidized metals as well as the oleophobicity of oxide surfaces are worth mentioning. Thermally grown oxide layer on aluminium alloy has been shown to exhibit hydrophobicity due to the roughness of the surfaces with varied morphology created through a thermal oxidation process [8]. The study revealed that the morphological changes occurring on the surfaces of the alloy due to the growth of vertical platelets of Al_2O_3 affected the hydrophobic behavior of the surfaces. It is these vertical Al_2O_3 platelets that forced a reduction in the contact area for the water drops resulting in a shift in the wetting behavior from the Wenzel state to the Cassie-Baxter state.

By applying a thermal oxidation and reduction cycle, superhydrophobicity has been achieved on a pure copper metal [9]. The morphological changes in the miniature structures of the copper nanowires formed during the thermal oxidation affected the water adhesion behavior effectively producing superhydrophobic copper surfaces. The superhydrophobicity of the surface was ascribed to

the alteration in the structure of the nanowires when they were reduced from CuO to Cu_2O.

High energy oxides have been used to achieve superoleophobic surfaces which have vast potential for underwater, anti-fouling applications. In this regard, copper oxide coating achieved on copper sheet through a simple chemical oxidative process exhibited superoleophobic behavior [10]. Also, oleophobicity of silicon oxide surfaces have been achieved through a microwave assisted reaction of fluorinated and aliphatic alcohols with the silicon oxide surfaces [11]. These alcohols used provided oleophobic monolayers on the SiO_2 surfaces and such oleophobicity were found to reduce as the alcohol content of the monolayers reduced. In the same vein, UV- irradiation has been used in a facile approach to generate oleophobicity in graphene oxide coatings [12]. The UV irradiation was used to gradually modify the chemistry and structure of the graphene oxide.

Lui and his co-workers [13] investigated clam shells, composed of $CaCO_3$ of their wettability to oils. It was noted that the shells' surfaces were superoleophobic in nature. This phenomenon of high underwater oil contact angle was attributed to the high energy $CaCO_3$ and the nanoscale roughness of the clam shells. Some other high energy materials such as nanoclay hydrogels have been coated on metal substrates to induce high contact angle of oil in underwater conditions.

Oleophobicity of Zn sheet surfaces roughened through immersion of the Zn sheets in hot deionized water has been reported [14]. The oleophobicity was ascribed to the growth of ZnO nanorods on the Zn sheet surfaces. The growth of the ZnO nanorods was found to be influenced by the variation in the immersion time. Also, a further concealing of the ZnO nanorods with fluorocarbon oligomers enhanced the wetting repellency properties of

---

Aniedi E. Nyong et al./ Ultraoleophobicity of Thermally Oxidized Surfaces of C36000 Alloy

the substrate. In the same vein, superhydrophobic and oleophobic surfaces have been demonstrated in Zn substrate using a combination of various methods namely; chemical etching, hydrothermal reaction and modification with fluorinated hydrocarbon [15]. The etching/hydrothermal reaction generated rough surfaces from which ZnO rods grew. These ZnO rods showed superhydrophobic and oleophobic behavior with distilled water and peanut oil respectively.

In this work, we will study the wetting behavior of oil, at the oil-water interface, on the surfaces of thermally oxidized C36000 alloy. The conditions of the thermal oxidation were varied and the influence of such variations on the contact angle of oil on the alloy surfaces studied.

Experimental

Materials
The C36000 alloy consisting of copper (61.70 wt. %), zinc (31.05 wt. %) and Pb (7.25 wt. %) was obtained from Badger Industries, Wisconsin, USA. The N_2-0.75 wt. % oxygen gas mix used for the thermal oxidation process was obtained from Praxair, Brookefield, USA.

Method
The samples of the C36000 alloy were prepared by cutting the alloy into sizes of 2.0 x1.0 x0.5mm. These cut samples were then polished in order to create smooth, fine surface finishing. The polishing step involved the use of silicon carbide papers of various grades, ranging from 400, 600, 1200 and 1600 grit-sizes. The final polishing step to achieve a smooth surface with the average surface roughness, R_a, of 0.1 microns was achieved by dipping a soft cloth in slurry of 0.1 micron alumina and then using it for the polishing of the samples' surfaces. This polishing process was done using a polishing machine (BeulerMetaserve 3000 model). The polished samples were then thoroughly washed in the ultrasonic bath, dried in air and stored in a dessicator.

The thermal oxidation process was done in different gaseous atmospheres, namely; N_2-0.75 wt. % O_2 gaseous atmosphere and in air. For the oxidation of the C36000 alloy in N_2-0.75 wt. % O_2 gaseous atmosphere, the furnace chamber was homogenized by the initial flow the N_2-0.75 wt. % O_2 gas mix through the furnace chamber at a rate of 4.5 liters per minute for five minutes, after which the samples were put into the inner chamber for the oxidation. The thermal oxidation in air was done at ambient conditions. In both cases , the temperature was set at 650° C and the thermal oxidation processes were carried out for different durations ranging from one to three hours. After the set time, the samples were removed and allowed to cool in the air-tight desiccator.

Characterization
The characterization involved surface morphology examination, average surface roughness evaluation, chemical composition determination and oil contact angle measurements at the oil-water interface. Examination of the surface morphology was done with the Hitachi-S4800 scanning electron microscope, set at high magnification under a 10.0 kV vacuum condition. The determination of the chemical composition of the oxidized surfaces of the samples was done through x-ray diffraction (XRD) as well

as through the energy dispersive x-ray (EDX) analyses respectively. The Scintag-2000 x-ray machine set at a 2θ range of 10°- 60° and at a continuous count rate of 2°/min., with the k_α-Cu emission of λ= 1.54°A was used to determine the chemical composition of the oxides and oxide phases formed on the thermal oxidation.

Further surface chemistry and analyses of the elemental composition of the oxidized samples was done with the aid of the energy dispersive x-ray probe installed in the Hitachi S-4800 scanning electron microscope. The average roughness of these surfaces, (R_a), was evaluated with a 2-D surface profilometer (phase II, SRG-4500 model). The R_a was determined over a cut off length λ of 5 microns. The measurement was done at five different places on the surfaces and the average values thereof calculated.

To characterize the wetting of these surfaces at the oil-water interfaces, the contact angle goniometer (Rame-Hart 250 model); with the drop shape image software was used. The drops of oil of about 5 µL were placed on the surfaces of the samples, submerged in water inside a transparent container, using a micro-syringe while they were submerged in water. For each sample, this was done for five times at five different spots on the surfaces and the average values of the contact angles calculated.

Results and Discussion
The results from the thermal oxidation of the C36000 alloy in the N_2-0.75 wt. % O_2 gas mix and in air in terms of the chemical composition of the oxidized surface layer, the surface morphology and thickness of the oxide layers as well as the contact angles of oil at the oil-water interface are as discussed.

X-ray diffraction and energy- dispersive X-ray analyses of the oxide layers
The x-ray diffraction peaks obtained for these samples before and after the thermal oxidation processes are shown in Figures 1 and 2 for the samples thermally oxidized in N_2-0.75 wt. % O_2 gaseous atmosphere and in air respectively. For the C36000 alloy samples thermally oxidized in N_2-0.75 wt. % O_2 gas mix, the miller indices of the major diffraction peaks were those of the (100), (002), (101), (102), (103) and (110) of the hexagonal ZnO planes on the basis of PDF card number 38–1477. Also, a very weak diffraction plane indexed as the (040) plane of PbO was noted.

The ease of formation of the ZnO oxide phase can be explained by comparing the values of the standard Gibbs free energies of formation of the oxides, $\Delta G°$. The following are the expected oxidation reactions and the corresponding standard Gibbs free energy of formation equations for the reactions , where T is the operational temperature of 650° C [16];

$$2\ Zn + O_2\ (g) \rightarrow 2\ ZnO \quad \Delta G° = -920400 + 396T \qquad (1)$$

$$4\ Cu + O_2\ (g) \rightarrow 2\ Cu_2O \quad \Delta G° = -346400 + 151.6T \qquad (2)$$

$$2Pb + O_2\ (g) \rightarrow 2\ PbO \quad \Delta G° = -208700 + 91.75T \qquad (3)$$
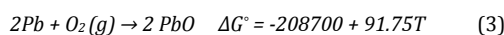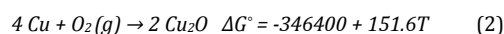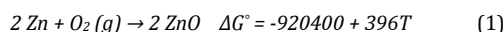
To this end , the ΔG for ZnO , Cu_2O and PbO from the equations are -633000 J, -247860 J and -149062 J respectively. The calculated values of ΔG confirmed that

the reaction of Zn with oxygen to form ZnO during the thermal oxidation process is the most spontaneous.

It should equally be noted that the presence of zinc in concentration greater than 20 % implies that whatever initial amount of copper oxides present are reduced by Zn such that ZnO becomes the only continuous oxide phase [17]. This aligns itself with these equations 4, 5 and 6 which describe the formation of ZnO:

$$Zn + \frac{1}{2}O_2 \rightarrow ZnO \qquad (4)$$

$$Zn + CuO \rightarrow ZnO + Cu \qquad (5)$$

$$Zn + Cu_2O \rightarrow ZnO + 2Cu \qquad (6)$$
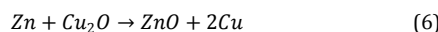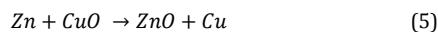
The x-ray diffraction peaks of the samples that were oxidized in air were comparable to those obtained from the diffraction analyses of the samples oxidized in N_2-0.75 wt. % O_2 gaseous atmosphere. The diffraction peaks were indexed as (100), (002), (102) and (110) planes of ZnO. The implication is that ZnO formed a continuous oxide layer after the thermal oxidation in air. However, the x-ray diffraction peaks were fewer as amount of oxygen present in the air was higher than that present in the N_2-0.75 wt. % O_2 gaseous atmosphere. This suggests a coarsening of the ZnO grains thus reducing the number of oxide planes available to diffract the x-rays.

The crystallite sizes of the ZnO was estimated using the full width at half maximum of the (100) peak using the Scherrer's formula [18]-

$$d = \frac{0.9\,\lambda}{\beta \cos\theta} \qquad (7)$$

The calculated grain sizes of the oxides were; 86 nm, 50.8 nm and 40.5 nm as well as 57.49 nm, 47.89 nm and 36.30 nm for the samples that were oxidized in N_2-075 wt. % O_2 gaseous atmosphere and in air for 1, 2 and 3 hours respectively. The oxide grains were smaller in sizes for the thermal oxidation done in air as compared to those done in N_2-075 wt. % O_2 gaseous atmosphere.

Beyond the x-ray diffraction analyses which confirmed a ZnO layer, the chemical composition of the oxidized samples were further appraised through the energy dispersive x-ray analyses, as shown in Figure 2 (a and b). From the EDX analyses of the surfaces, it was noted that considerable amount of oxygen molecules were incorporated in the surfaces.

The EDX analyses showed that zinc pre-dominated the surfaces as can be seen in the higher counts as quantified in the EDX spectra. However, Cu and Pb were also present in limited quantities, especially at early periods of the thermal oxidation in N_2-075 wt. % O_2 gas mix. The trace amounts of Cu and Pb are from the base alloy and also from the fact that the relatively lower melting point of lead compared to the other alloying elements meant that at these early stages of the thermal oxidation, the discretely distributed Pb granules at grain boundaries melted easily and segregated to the surfaces where they were oxidized. Lead melts at 327.5℃ [19]. However, we expect that as the thermal oxidation progressed, any PbO formed at the early stages are reduced by Zn to form ZnO as a continuous oxide layer.

(a)

(b)
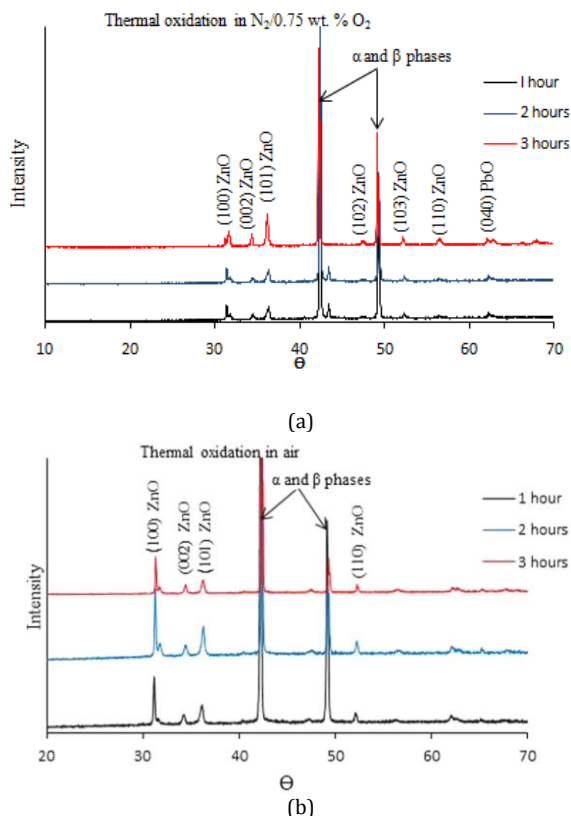
Figure 1: X-ray diffraction planes of oxide layers in (a) N_2-0.75 wt. % O_2 gaseous atmosphere and (b) air after thermal oxidation for 1, 2 and 3 hours
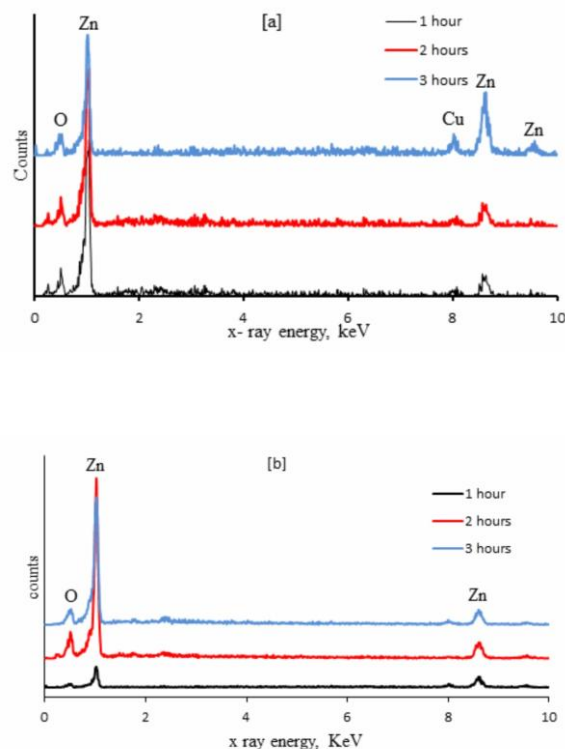
Figure 2: Energy dispersive x-ray analysis of oxide layer after oxidation in (a) N_2/0.75 O_2 wt. % gas mix and (b) air for 1, 2 and 3 hours
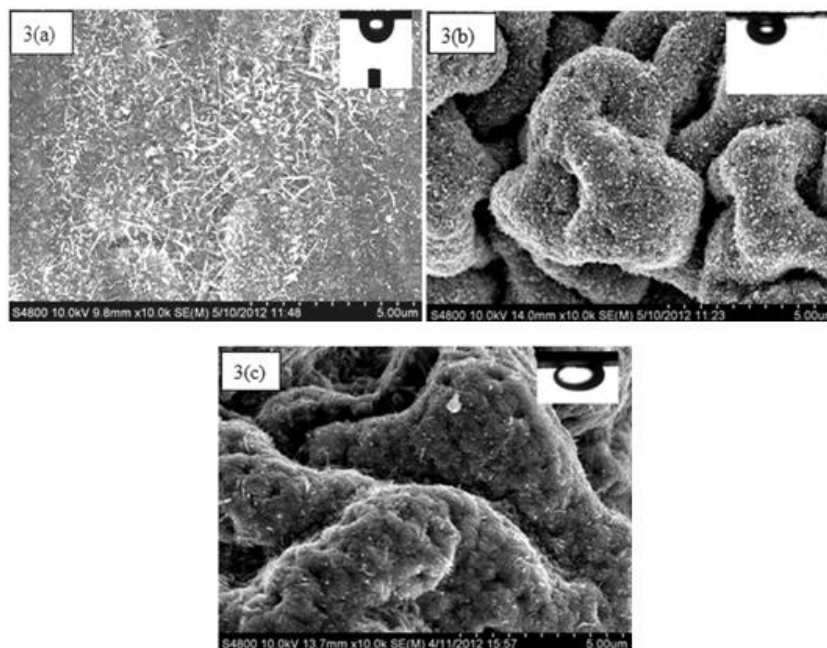
Figure 3: SEM images of C36000 alloy oxidized in N_2-0.75 wt. % O_2 gas atmosphere for (a) 1 hour, (b) 2 hours, and (c) 3 hours. (insert is image of oil drop)
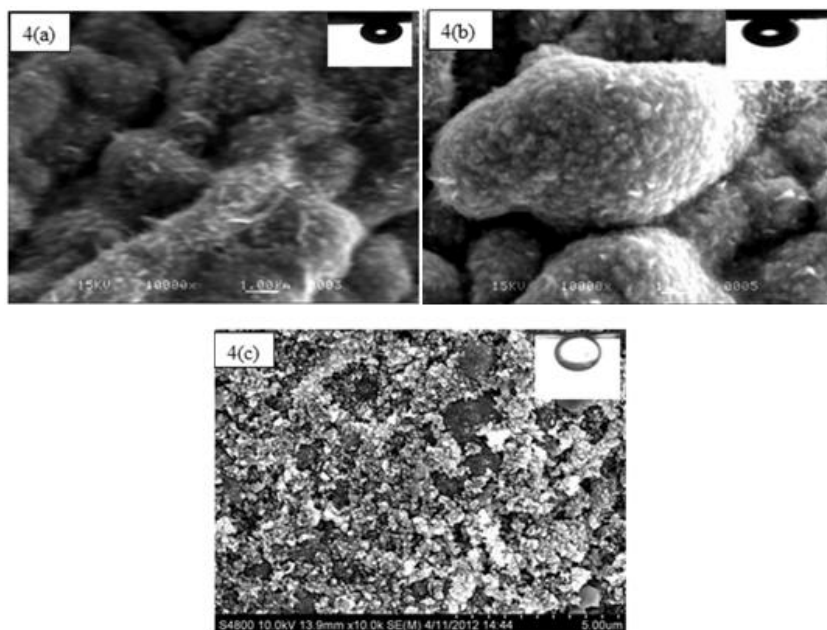
Figure 4: SEM images of C36000 alloy oxidized in air for (a) 1 hour, (b) 2 hours, and (c) 3 hours. (Insert is image of oil drop)

Surface morphology examination

The examination of the SEM images showed that the surfaces consisted of the oxide granules as well as some nanowires in few instances. The sizes of these oxide granules remained in the nanometric scale irrespective of the time and gaseous medium involved in the thermal oxidation process. The oxide morphology revealed severe contortion and distortion of the surface layer. Therefore grooves were quite conspicuous from the SEM images.

The linear expansion coefficients of the alloy and ZnO are $20.5^{\times}10^{-6}$ C^{-1} (at 20° C) and $4.31^{\times}10^{-6}$ K^{-1}/ $2.49^{\times} 10^{-6}$ K^{-1} for α_a/α_c [20] respectively. Using these values, we estimated the volume expansion expected of the alloy and

the continuous layer of ZnO, using the relationship $3\alpha\Delta T$; with α = linear expansion coefficient and ΔT = change in the temperature of the process (from ambient room temperature to process temperature of 650° C).

The ZnO showed smaller volume expansion values of $8.15^{\times}10^{-3}$ and $4.71^{\times}10^{-3}$ on the a- and c-axes of the oxide respectively, compared to a volume expansion of $3.80^{\times}10^{-2}$ for the alloy. The contortions of the oxide layers were therefore due to substantial stress build-up at the alloy-oxide interface due to these differences in the volume expansion of the oxide and the bulk alloy.

Other factors such as differences in the crystallographic structure as well as in the densities of the alloy and the

oxides formed in the oxide layer may equally have some influence on the oxide layer contortions [21-22]. Spalling along the oxide-alloy interface did not occur at the temperature in which the thermal oxidation was done.

Beyond the contortion of the surfaces, the thickness of the oxide layers showed direct dependence on the amount of oxygen used in the thermal oxidation process. The samples oxidized in N_2-0.75 wt. % gaseous atmosphere formed thinner oxide layers compared to the samples that were oxidized in air. This to some extent explains the lesser level of contortion of the oxide layers formed on samples that were thermally oxidized in air; as we believe that the thicker oxide layers provided larger surface volumes for the dissipation of stresses built up during the thermal oxidation process. The oxide layer thickness values recorded are stated in Table 1.

The oxide layer for the samples oxidized for 1 hour in the 0.75 wt. % O_2 gas showed a high density of oxide nanowires. The nanowire density was estimated as an average of 19 nanowires per μm^2. The surface density of the nanowires diminished totally when the oxidation time was extended to two and three hours respectively, as nanowire growth was not observed at these oxidation times. Beyond the contortions observed, the built-up stresses prevalent at the oxide - C36000 brass interface equally assisted in the growth of the nanowires.

The x-ray diffraction energy dispersive (EDX) spot analysis of an individual nanowire, marked x in Figure 5, showed that it was chiefly composed of zinc and oxygen in a compositional ratio of 80.50 wt. % of zinc and 19.50 wt. % of oxygen respectively. This confirmed the nanowires as being ZnO, as previously noted from the x-ray diffraction of the oxide layer.

The growth of the ZnO nanowires is based on a diffusion mechanism, where the Zn in the form of Zn^{2+} ions diffuse outwardly towards the surface from the oxide-C36000 alloy interface while the oxygen ions diffuse towards the interface in the opposite direction. At close view of the nanowires at very high magnification of 50 000x, the ZnO nanowires were found to grow out of the nucleated oxide grains directly as shown in Figure 5. The growth of the nanowires from the ZnO grains at the 1 hour thermal oxidation window implies that being the thinnest of the oxide layers, it experienced marked deformation which led to an increase in the dislocation density in the oxide scale thereby favoring the ZnO nanowire growth [23-25].

(a)

(b)
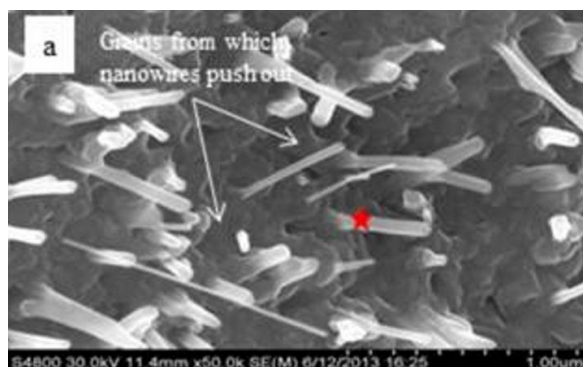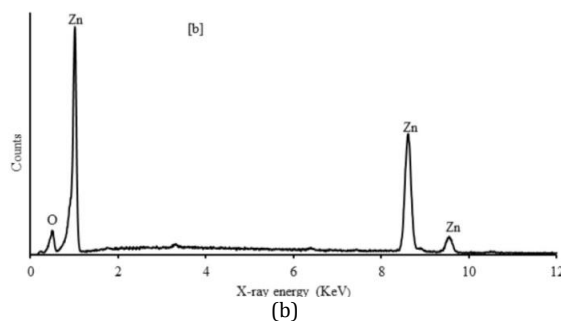
Figure 5: (a) SEM showing the growth of ZnO based directly from oxide grains (b) EDX spot analysis of the chemical composition of the nanowire marked x in a

The dislocations around the edges of the oxide grains serve as vents for the diffusion of Zn^{2+} ions to the surface and continuous oxidation by O^{2-} ions for the growth of the observed nanowires.

Contact angle of oil evaluation

The contact angle of oil at the oil-water interface showed a dependency on the nature and morphology of the oxide formed during the thermal oxidation process. These values so measured as well as the average surface roughness of the samples are presented in Table 1.The average surface roughness values, given by R_a were observed to generally increase as the oxidation times and the amount of oxygen in the oxidizing atmospheres were altered to higher values. The average surface roughness is the arithematic average value of the deviation of a surface topology above and below a given center line [26]. Therefore, the increase in the average roughness with time can be ascribed to the increased severity of the contortion of the oxide layer as well as the increased presence of oxide grains that are in the nanometric scale as the oxidation time and the amount of oxygen in the oxidizing atmospheres are increased.

Table 1: Table showing R_a, oxide layer thickness and contact angle of oil for C36000 alloy thermally oxidized in N_2/0.75 wt. % O_2 gas atmosphere and in air

Oxidizing atmosphere	Oxidation time (hours)	R_a (μm)	Oxide layer thickness (μm)	f_{so}	Contact angle of oil, θ
No oxidation	0	0.1	--------	-------	53.0° ± 1.1°
N_2/0.7 wt. % O_2	1	0.28	4.4 ± 0.3	0.85	68.2° ± 9.7°
	2	0.42	5.2 ± 0.8	0.44	106.9° ± 8.8°
	3	0.62	7.0 ± 1.4	0.37	113.9 ± 1.9
Air	1	0.48	28.3±3.5	0.45	105.8° ± 3.2°
	2	0.52	40.2±1.9	0.34	116.7° ± 4.6°
	3	0.64	47.7±4.6	0.21	130.9° ± 1.9°

The nature of the oxides influenced the fractional surface areas available for wetting at the oil-water interface. From the dimensions of the oxide grains and the ZnO nanowires stated earlier, it is expected that the fractional surface area (f_{so}) of these surface were very low. The relationship in equation 8 was used to estimate the fractional surface area (f_{so}) of ZnO nanowires, which grew on the samples that were thermally oxidized for 1 hour in N_2/0.75 wt. % O_2 gas mix

$$f_{so} = \frac{A_{sl}}{A_{proj.}} = \frac{X}{W+X} \qquad (8)$$

In the equation, w is the distance between the nanowires and x is the average diameter of the nanowires. In this case, the average length, average diameter and the average distance between the nanowires were estimated as 0.52 ± 0.31 μm, 34.0 ± 0.02 nm and 0.17 ± 0.07 nm respectively. To this end, the value of f_{so} estimated thereof was lesser than 1, with a value of 0.17.The value is quite smaller than that estimated from [9] and stated in Table 1. This implies that other factors beyond the low f_{so} influenced the underwater coil contact angles.

Beyond the very low f_{so} estimated for the surfaces on which the ZnO nanowires grew, the oxide grains being very small in sizes equally conveyed low values of f_{so} on the oxide layers. As stated earlier, the increased amount of oxygen during the thermal oxidation of the alloy in air resulted in the generation of smaller oxide grains as estimated from the XRD studies. These reduced sizes of the oxide grains implied low f_{so} which caused the oil contact angles shifting to higher values. Furthermore, surface tension of oil and other organic liquids are known to be generally of lower values than that of water [27]. It is expected that the oxide surfaces will, beyond exhibiting low f_{so}, have high-energy due to surface tension phenomena. The two factors of low f_{so} and surface tension phenomenon at the oil-water interface is therefore responsible for the underwater oil contact angle behavior.

Thus, the factors of low fractional area available for the wetting and the surface tension phenomena at the oil-water interface are the main reasons for the ultraoleophobic behavior of the thermally oxidized samples under water. The contact angle of oil increased with increase in the thermal oxidation time as well as with increase in the amount of oxygen in the oxidizing atmosphere as shown in Figure 6.
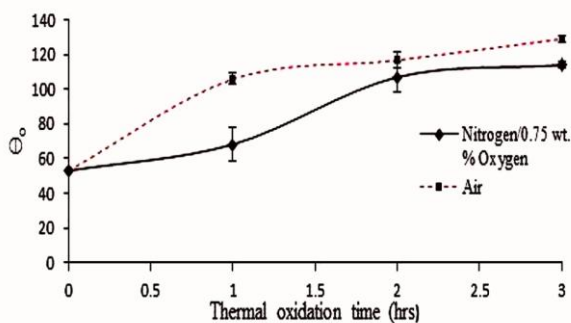
Figure 6: Plot of the underwater contact angle of oil (θ_o) against the oxidation time (in hours)

In this context, we use the Cassie-Baxter model, given in equation 9 [28] to calculate the fractional surface area values, based on the measured underwater oil contact angle values on the thermally oxidized surfaces (θ_o) and the underwater oil contact angle on the polished, unoxidized C36000 copper alloy surface ($\theta = 53.0° \pm 1.1°$).

$$cos\,\theta_o = f_{so}(cos\,\theta + 1) - 1 \qquad (9)$$

The calculated values stated in Table 1 showed that these values diminished as the oxide granules reduced in their sizes, as represented in Figure 7.
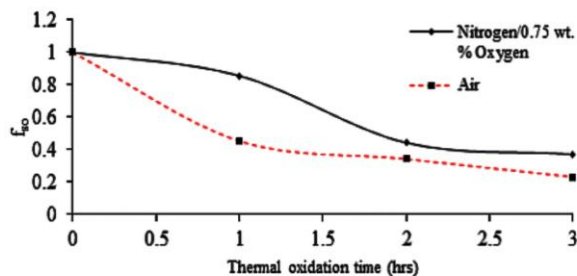
Figure 7: Plot of the fractional surface area (f_{so}) available for the wetting by oil drops against the thermal oxidation time

The increase in the thickness of the oxide layers further conveyed additional basis towards a sustainable Cassie-Baxter state for ultraoleophobicity. Essentially, the thicker oxide layers served , more effectively, as water traps which further reduced the surface area of the solid-oil interface needed for increase in the oil contact angles [29].

With changes in the morphology of the oxide surface layer on the C36000 copper alloy as well as the oxide layer thickness, the oil contact angles increased at the oil-water interface. The ultra-oleophobicity observed with increase in the thermal oxidation time and oxygen weight per cent in the oxidizing atmospheres is therefore influenced by the presence of contortions within the layer that effectively trapped water thereby sustaining a Cassie-Baxter wetting state for the ultraoleophobicity.

Conclusions

The thermal oxidation of the C36000 copper alloy generated a hierarchical oxide layer that was composed of nanowires and oxide grains of nanometric sizes. The SEM images of the oxide layers further confirmed severe convolution or contortion of these layers. Furthermore, the chemical composition of the oxide layers, determined through x-ray diffraction analyses and energy dispersive x-ray analyses, showed that they consisted of ZnO. The contact angles of oil measured under water showed consistent increase in values until 130.9^0 confirming ultraoleophobicity.

These values for the contact angles of oil were influenced by the convolution of the oxide layer, the reduction in the surface wetting area covered by the nanometric oxide grains, increasing surface roughness and the high energy of the oxide layers. These factors influenced the contact angles of oil under water by shifting them towards higher values.

References

1. Davies, J. R., ASM Specialty Handbook- Copper and Copper Alloys, ASM International, 2001, 153-167.
2. Pantazopoulos, G., Vazdirvanidis, A., 'Characterization of the Microstructural Aspects of Machinable α-β Phase',BrassMicroscopy and Analysis, 2008, 22, 13-16.
3. Ozgonicz, W., Kalinowska-Ozgowicz, E., Graegorczyk, B.,'The Microstructure and Mechanical properties of the alloy Cu70Zn30 after recrystallization annealing',Journal of Achievement in materials and Manufacturing Engineering, 2010, 40, 79-82.
4. Kundig, K. J. A., Copper and Copper Alloys. In M. Kutz ed. Handbook of Materials Selection, John Wiley & Sons, Inc., 2002, 135-200.

5. Savantt, S. S., Khandeparker, D., Tulaskar, A., Venkat, K., Garg, A., 'Corrosion and microfouling of copper and its alloys in tropical marine waters of India (Mangalore)', Indian Journal of Chemical Technology, 1995, 2, 322-326.

6. Hejazi, V.,Nosonovsky, M., 'Wetting transitions in two-, three- and four- phase system',Langmuir, 2011, 28, 2173-2180.

7. Hejazi, V., Nyong, A. E., Rohatgi, P. K., Nosonosky, M., 'Wetting transitions in underwater oleophobic surface of brass', Advanced Materials, 2012, 24, 5963-5966.

8. Samad, J. E., Nychka, J. A.,'Wettability of biomimetic thermally grown aluminum oxide coatings', Bioinspiration and Biomimetics, 2010, 6, 1-9.

9. Lee, S. M., Kim, K. S., Pippel, C., Kim, S., Kim, J-H., Lee, H-J, 'Facile Route Toward Mechanically stable Supehydrophobic Copper using Oxidation-Reduction induced morphology changes', Journal of Physical Chemistry C, 2012, 116, 2781 – 2790.

10. Ling, L., Mingjie, L., Peipei, C., Ma, J., Han, D., Jiang, L., 'Bio-Inspired Hierarchical Macromolecule- Nanoclay Hydrogels for Robust underwater superoleophobicity', Advanced Materials, 2010, 22, 4826-4830.

11. Lee, A. W. H., Gates, B. D., 'Tuning oleophobicity of Silicon Oxide Surfaces with mixed monolayers of Aliphatic and fluorinated Alcohols',Langmuir, 2016, 32, 13030-13039.

12. Li, H., Huang, Y., Mao, Y., Xu, W. L., Ploehn, H. J., Yu, M., 'Tuning the underwater oleophobicity of graphene oxide coatings via UV irradiation' Chemical Communication, 2014, 50, 9849-9851.

13. Liu, X., Zhou, J., Xue, Z., Gao, J., Meng, J., Wang, S., Jiang, L., Clam's shell inspired high-energy inorganic coatings with underwater low adhesive superoleophobicity. Advanced Materials, 2012, 24, 3401–3405.

14. Khedir, K. R., 'Superhydrophobic and Highly oleophobic zinc sheet surfaces Developed by a Simple Technique',Journal of Materials Science and Engineering B, 2016, 6 (7-8), 179-188.

15. Hao, L., Yu, S., Han, X., Zhang, S., 'Design of submicron structures with superhydrophobic and oleophobic properties on zinc substrate', Materials & Design, 2015, 85, 653–660.

16. Gaskell, D. R., Introduction to the Thermodynamics of Materials Taylor and Francis, 2003, 584-585.

17. Hauffman, K., Oxidation of Metals, Plenum Press, New York, 1965, 288.

18. Bindu, P., Thomas, S., 'Estimation of lattice strain in ZnO nanoparticles: X-ray peakprofile analysis', Journal of Theoretical and Applied Physics, 2014, 8, 123-134.

19. Lide D. R., CRC Handbook of Chemistry and Physics 88th Edition, CRC Press, 2007,12-219.

20. V. A Coleman and C. Jagadish. Basic properties and applications of ZnO. In: ChennupatiJagadish and Stephen J. Pearton, eds. Zinc Oxide, Bulk, Thin Films and Nanostructures, Processing, Properties and Applications. Elsevier; 2006, 1-20.

21. Xu , C. H., Zhu, Z. B., Li, G. L.,Xu, W. R., Huang, H.X., 'Growth of ZnO nanostructure on Cu0.62Zn0.38 brass foils by thermal oxidation',Materials Chemistry and Physics, 2010, 124, 252–256.

22. Xu, C H, Zhu, Z B, Lui, H F, Surya, C, Shi, S. Q., 'The effect of Oxygen partial pressure on the growth of ZnO nanostructure on Cu0.62Zn0.38 brass during thermal oxidation', Superlattices and microstructures, 2011, 49, 408-415.

23. Khanlary, M. R., Vahed, V., Reyhani, A., 'Synthesis and characterization of ZnO nanowires by thermal oxidation of Zn Thin Films at various Temperatures', Molecules, 2012, 17, 5021-5029.

24. Yuan, L., Wang, C., Cai, R., Wang, Y., Zhou, G., 'Spontaneous ZnO nanowire Formation during oxidation of Cu-Zn alloy', Journal of Applied Physics, 2013, 114, 023512.

25. Yuan, L., Wang, Y.Q., Mema, R., Zhou, G.W., 'Driving force and growth mechanism for spontaneous oxide nanowire formation during the thermal oxidation of metals',ActaMaterialia, 2011, 59, 2491–2500.

26. Bhushan, B., Introduction to Tribology, John Wiley and Son, 2002, pp. 18-19.

27. Brown, P. S., Bhushan, B., 'Designingbioinspired superoleophobic surfaces', APL Materials, 2016, 4, 1-11.

28. Cassie, A.B.D.; Baxter, S., 'Wettability of porous surfaces', Transactions of the Faraday Society, 1944, 40, 546–551.

29. Nyong, A. E., Rohatgi, P. K., 'Underwater superoleophobicity induced by the thickness of the thermally grown porous oxide layer on C84400 Copper alloy', Applied Sciences, 2014, 4, 42-54.